Effects of transient bottom water currents and oxygen concentrations on benthic exchange rates as assessed by eddy correlation measurements

Moritz Holtappels,[1] Ronnie N. Glud,[2,3,4] Daphne Donis,[1] Bo Liu,[1] Andrew Hume,[5] Frank Wenzhöfer,[1,6] and Marcel M. M. Kuypers[1]

Received 17 October 2012; revised 1 February 2013; accepted 5 February 2013; published 12 March 2013.

[1] Eddy correlation (EC) measurements in the benthic boundary layer (BBL) allow estimating benthic O_2 uptake from a point distant to the sediment surface. This noninvasive approach has clear advantages as it does not disturb natural hydrodynamic conditions, integrates the flux over a large foot-print area and allows many repetitive flux measurements. A drawback is, however, that the measured flux in the bottom water is not necessarily equal to the flux across the sediment-water interface. A fundamental assumption of the EC technique is that mean current velocities and mean O_2 concentrations in the bottom water are in steady state, which is seldom the case in highly dynamic environments like coastal waters. Therefore, it is of great importance to estimate the error introduced by nonsteady state conditions. We investigated two cases of transient conditions. First, the case of transient O_2 concentrations was examined using the theory of shear flow dispersion. A theoretical relationship between the change of O_2 concentrations and the induced vertical O_2 flux is introduced and applied to field measurements showing that changes of 5–10 μM O_2 h^{-1} result in transient EC-fluxes of 6–12 mmol O_2 m^{-2} d^{-1}, which is comparable to the O_2 uptake of shelf sediments. Second, the case of transient velocities was examined with a 2D k-ε turbulence model demonstrating that the vertical flux can be biased by 30–100% for several hours during changing current velocities from 2 to 10 cm s^{-1}. Results are compared to field measurements and possible ways to analyze and correct EC-flux estimates are discussed.

Citation: Holtappels, M., R. N. Glud, D. Donis, B. Liu, A. Hume, F. Wenzhöfer, and M. M. M. Kuypers (2013), Effects of transient bottom water currents and oxygen concentrations on benthic exchange rates as assessed by eddy correlation measurements, *J. Geophys. Res. Oceans*, *118*, 1157–1169, doi:10.1002/jgrc.20112.

1. Introduction

[2] In sediments underlying well oxygenated bottom waters, O_2 is the ultimate electron acceptor of almost all electron equivalents released during the oxidation of organic matter [*Canfield et al.*, 2005; *Thamdrup and Canfield*, 2000]. O_2 uptake of the sediment is therefore used as a robust proxy for benthic carbon mineralization [*Glud*, 2008]. Common approaches to measure the benthic O_2 uptake include O_2 microsensor profiles of surface sediments [*Jørgensen and Revsbech*, 1985] and incubations of sediment and overlying water in closed systems such as in situ chamber incubations [*Glud et al.*, 1995]. The two approaches are complementary: O_2 microsensor profiles consider the diffusive uptake, while the chamber approach includes convective contribution from bioirrigation; therefore, paired deployments allow assessment on the fauna mediated O_2 exchange [*Glud*, 2008; *Wenzhöfer and Glud*, 2002]. The incubation approach is, however, strongly invasive, and natural hydrodynamic conditions in the enclosed incubation volume are difficult to mimic, which can have severe affects not only on the O_2 transport in permeable sediments [*Huettel et al.*, 1996], but also on O_2 transport across the diffusive boundary layer above cohesive sediments [*Glud et al.*, 2007; *Lorke et al.*, 2003].

[3] In 2003, the eddy correlation (EC) approach was adapted from atmospheric sciences [*Berg et al.*, 2003] as an alternative way to estimate benthic fluxes. The method relies on natural hydrodynamic conditions as it measures the turbulent transport of O_2 a few centimeters above the sediment water interface, in the so-called benthic boundary

[1]Max Planck Institute for Marine Microbiology, Bremen, Germany.
[2]University of Southern Denmark, Nordic Centre for Earth Evolution, Odense M, Denmark.
[3]Scottish Association for Marine Science, Scottish Marine Institute, Oban, UK.
[4]Greenland Climate Research Centre, Nuuk, Greenland.
[5]Global Environment Facility, Washington, DC, USA.
[6]HGF-MPG Bridge Group for Deep Sea Ecology and Technology, Alfred-Wegener-Institute for Polar and Marine Research, Bremerhaven, Germany.

Corresponding author: M. Holtappels, Max Planck Institute for Marine Microbiology, Celsiusstrasse 1, 28359 Bremen, Germany. (mholtapp@mpi-bremen.de)

2169-9275/13/10.1002/jgrc.20112

layer (BBL). EC measurements combine high frequency measurements of flow velocities and O_2 concentrations in the same sampling volume, from which the instantaneous O_2 flux and a time averaged O_2 flux can be calculated. The EC approach combines several significant advantages: (1) because of its noninvasive nature, the EC approach allows continuous measurements to monitor the response of benthic O_2 uptake on changing environmental conditions [*Hume et al*., 2011]; (2) it is not confined by boundary interface conditions and allows to investigate O_2 sinks and sources at boundaries such as hard bottom substrate [*Glud et al*., 2010], sea ice [*Long et al*., 2011] and sandy sediments [*Reimers et al*., 2012]; (3) it integrates the flux across a large surface area [*Berg et al*., 2007] and thus integrates small to mesoscale heterogeneity of many benthic environments. These essential advantages initiated many studies on the boundary layer flux of other scalars such as dissolved nitrogen and phosphate [*Holtappels et al*., 2011], nitrate [*Johnson et al*., 2011], salinity [*Crusius et al*., 2008] and density [*Holtappels and Lorke*, 2011]. However, the downside of the EC approach is the complex data processing and interpretation, which requires knowledge in time series analysis and hydrodynamics. O_2 fluxes from EC measurements often show extensive short-term variability [*Lorrai et al*., 2010] that is poorly explained by benthic community response. So far, robust criteria to validate these fluxes are missing. It is therefore necessary to identify and quantify errors caused by sensor limitations such as slow response times and low signal to noise ratios as well as errors introduced by the hydrodynamic settings. Here, we focus on hydrodynamic conditions, which induce fluxes in the BBL that add to the true benthic flux estimate. It is useful to distinguish between the O_2 flux across the sediment-water interface and the flux at the sensor position, usually situated at 15–25 cm above the sediment. These fluxes should be identical if we can assume [*Baldocchi*, 2003; *Loescher et al*., 2006; *Lorrai et al*., 2010]: (1) negligible reaction rates in the water layer between sediment and measuring position; (2) a constant surface roughness of the measuring site, and unobstructed flow field ensuring uniform turbulent diffusivity upstream; (3) steady state (i.e., time invariant) mean current velocities, and; (4) steady state mean O_2 concentrations. If these assumptions are not met, the flux at the sensor position can significantly deviate from the flux across the sediment-water interface. The first assumption usually holds as the integrated O_2 consumption rates in the water layer below the sensor position are 1–2 orders of magnitude lower than benthic O_2 fluxes. The second assumption can be reviewed by additional observations from sediment sampling or video surveys, whereas the steady state assumptions for mean current velocities and mean O_2 concentrations can be evaluated from the EC measurement itself. In this study, the validation of the assumption of steady state concentrations and steady state velocities for typical coastal settings is examined and discussed on the basis of two case studies. *Case study 1*: Based on the theory of shear flow dispersion [*Fischer*, 1979; *Taylor*, 1953], we introduce a theoretical relationship between the temporal change of concentrations and the induced vertical flux. We present EC measurements from the Black Sea that are clearly affected by transient (i.e., nonsteady state) O_2 concentrations and validate the applicability of the analytical model. *Case study 2*: A 2D k-ε turbulence model is used to quantify the effect of transient velocities on the EC-flux. EC-measurements from a tidally influenced fjord (Loch Etive, Scotland) that show strong correlation between velocity and EC-flux are analyzed and compared with the numerical model.

2. Theory and Methods

2.1. Case Study 1—Transient O_2 Concentrations

[4] Water masses that move along the sediment can have different origins and can therefore carry different O_2 concentrations. Especially in stratified coastal seas and lakes, sediments intersect with the oxycline of the water column and are therefore exposed to waters with significant O_2 gradients. These water masses move along the sediment with mean current velocities that are decreasing towards the sediment (Figure 1a). The differential advection of water masses with a concentration gradient in the stream-wise direction will cause a vertical concentration gradient and thus a vertical flux (Figure 1b).

2.1.1. The Analytical Model

[5] The balance between differential advective transport in the streamwise direction and diffusive transport in the vertical direction is expressed according to *Fischer* [1979]:

$$\frac{\partial}{\partial z} D_t(z) \frac{\partial C'}{\partial z} = U' \frac{\partial \bar{C}}{\partial x} \tag{1}$$

where D_t denotes the turbulent diffusion coefficient. Here, the concentrations (C) and current velocities (U) are decomposed

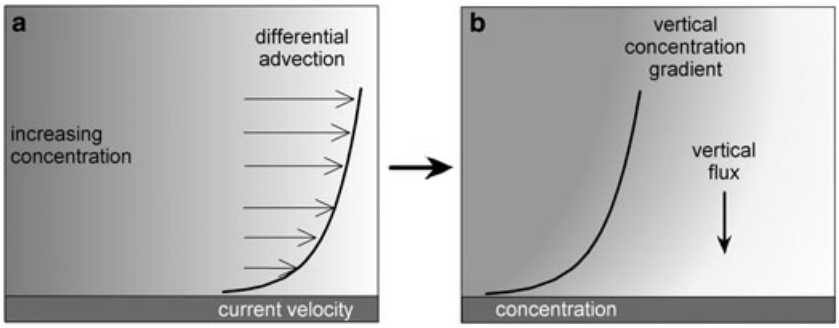

Figure 1. Schematic drawing of the flux caused by nonsteady state concentrations. Differential advection of horizontal concentration gradients (a) cause vertical gradients and (b) a vertical flux, which adds to the flux across the sediment water interface.

into depth averaged values and their deviations $C(x,z) = \bar{C}(x) + C'(x,z)$ and $U(z) = \bar{U} + U'(z)$ where x and z denote the streamwise and the vertical directions, respectively, and U is assumed to be uniform in the streamwise direction.

[6] The interaction between differential advection and vertical diffusion is known as shear flow dispersion. This phenomenon was first described by *Taylor* [1953], who initiated many studies on the spreading of contaminants in conduits and rivers. For a thorough description of shear flow dispersion, we refer to *Fischer* [1979]. In this study, we focus on the induced vertical flux in the BBL, which adds to any flux across the sediment water interface. For simplicity, we assume in the following zero flux at the bottom ($z = 0$). Then integration of equation (1) gives the vertical diffusive flux

$$J(z) = D_t(z)\frac{\partial C'}{\partial z} = \frac{\partial \bar{C}}{\partial x}\int_0^z U'(z)\mathrm{d}z \tag{2}$$

[7] Given Taylor's frozen turbulence assumption [*Taylor*, 1938], the concentration gradient in the streamwise direction, $\partial\bar{C}/\partial x$, can be expressed by the change of concentration over time divided by the mean current velocity, $(\partial C/\partial t)/\bar{U}$, so that equation (2) is rearranged to

$$J(z) = \frac{\partial C}{\partial t}\frac{1}{\bar{U}}\int_0^z U'(z)\mathrm{d}z \tag{3}$$

[8] In a fully developed turbulent flow, the logarithmic law of the wall (log-law) [*von Karman*, 1930] gives estimates of the current velocity profile

$$U(z) = \frac{u_*}{\kappa}\ln\left(\frac{z}{z_0}\right) \tag{4}$$

where u_* and z_o denote the shear velocity and the hydraulic roughness, respectively. Applying the log-law for the velocities in equation (3), we derive (see Appendix A for details)

$$J(z) = \frac{\partial C}{\partial t} z \frac{\ln(z/z_{up})}{\ln(z_{up}/z_0) - 1} \tag{5}$$

with z_{up} as the upper boundary of the BBL. The logarithmic expressions on the right side of equation (5) give negative values. Thus, concentrations that increase over time cause negative (downward) fluxes (Figure 1), and decreasing concentrations cause positive (upward) fluxes. It is evident from equation (5) that the vertical flux caused by transient concentrations is independent from the current velocity. Below, equation (5) is used to estimate the induced vertical flux derived from in situ data. From the time series of the in situ EC measurement, the change of concentration over time, $\partial C/\partial t$, was calculated, and the position z of the EC measuring volume was well constrained. The length scales z_{up} and z_o can be extracted by fitting equation (4) to measured velocity profiles (see below). If the velocity profile is not known, z_o can be calculated directly from equation (4), since U and u_* can be estimated from ADV data [*Inoue et al.*, 2011]. This procedure can be applied to most EC datasets.

2.2. Case Study 2—Transient Current Velocities

[9] In a turbulent steady state boundary layer flow, the profile of mean O_2 concentration depends on the turbulent diffusivity in the BBL and on the upper and lower boundary conditions, i.e., the flux across the sediment water interface and the O_2 concentration at the upper boundary of the BBL (Figure 2). The turbulent diffusivity depends on several factors such as bottom roughness, density stratification and flow velocity [*Holtappels and Lorke*, 2011]. For the sake of simplicity, and because flow velocity is the most dynamic factor, we only focus on the effect of transient current velocities on turbulent diffusivity and subsequently on the O_2 flux. Assuming constant boundary conditions, a change in current velocity over time will cause a change of the turbulent diffusivity and thus an adjustment of the O_2 concentration profile (Figure 2). Any adjustment of the O_2 concentration profile is ultimately linked to an O_2 flux in the bottom water that adds to the O_2 flux from benthic O_2 uptake. Increasing current velocities will cause the erosion of O_2 concentration gradients and increase the O_2 flux in the downward direction, whereas decreasing current velocities cause the buildup of concentration gradients and decrease the O_2 flux in the downward direction. It should be noted that the flux across the sediment-water interface is irrelevant for the induced flux in Case 1, but determines the induced flux in Case 2. If the O_2 flux across the sediment-water interface is positive (benthic primary production), the induced O_2 flux will change direction as well.

2.2.1. The Numerical Model

[10] Using the finite element program COMSOL Multiphysics® 4.3 (www.comsol.com), the turbulent boundary layer flow and the O_2 transport was modeled in a 2D channel of 6 m length and 1.5 m height. Within COMSOL, the low-Reynolds-number k-ε turbulence model was applied (see Appendix B for details), which uses dampening functions to solve for the region close to the wall, where viscous forces dominate. This allows the use of no slip boundary condition instead of wall functions [*Abe et al.*, 1994]. The k-ε turbulence model was coupled with a convection-diffusion model (see Appendix B for details) using the following domain and boundary settings. In the k-ε model, no slip boundary conditions were used

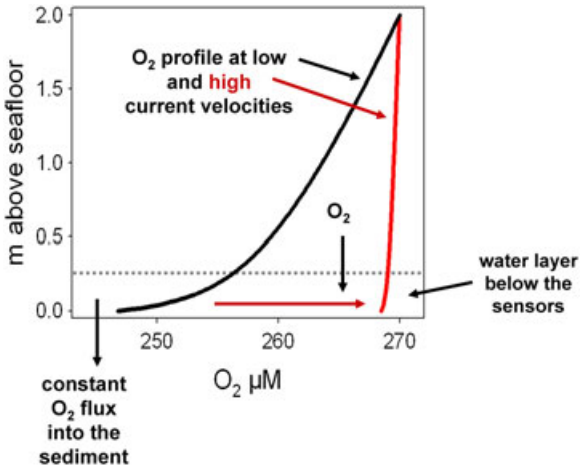

Figure 2. Schematic drawing of the flux caused by nonsteady state current velocities. Here, accelerating flow causes a vertical flux into the layer below the sensor (indicated by the horizontal line), which adds to the flux across the sediment water interface.

for the lower boundary, the upper boundary was set to symmetry condition, the left and right boundary were set to periodic boundary conditions, thus the variables solved for have the same value at the inflow and outflow boundary. In this way, an infinite long boundary flow could be simulated. Fluid motion was forced by a pressure gradient between the left and right boundaries. The pressure gradient was manually adjusted to give the intended velocity change. The pressure gradient was changing with time, thus forcing a transient current velocity. In the convection diffusion model, the upper boundary was set to a fixed O_2 concentration of 300 μM, whereas the lower boundary was set to a constant O_2 flux of -10 mmol m^{-2} d^{-1} to evaluate effects on a constant realistic background level. The left and right boundaries were set to periodic boundary conditions thus concentrations at the inflow boundary were taken from the outflow boundary. The output of the k-ε model, i.e., the velocity field and the turbulent viscosity, were used as input for the convective and diffusive transport. The coupled model was solved for a period of 14 h using a time dependent solver. Furthermore, the COMSOL model was used to estimate the deviation of the EC flux from the benthic O_2 uptake based on an EC deployment at Loch Etive, Scotland. For this, the pressure gradient in the model was adjusted to meet the measured current velocities, the EC flux measured in situ over 56 h was averaged and used as a lower boundary condition, and an average O_2 concentration of 170 μM was used as upper boundary condition.

2.3. Field Measurements

[11] Eddy correlation measurements were conducted at two different locations. Site 1 (for Case study 1) was located on the Crimean shelf, Black Sea, where O_2 dynamics were studied as part of the EU project HYPOX. During a cruise with the RV MS Merian in April/May 2010 a moored EC system was deployed for 14 h at 135 m depth (44°38.84′N, 33°0.18′E). At this depth, the oxycline intersects with the sediment, causing variable O_2 concentrations between 10 and 150 μM, as measured from a nearby mooring. The EC measurement at this site is therefore ideal for evaluating effects of transient O_2 concentrations on EC flux estimates. Video surveys and sediment coring were used to characterize the sediment as homogenous fine grained mud with no signs of benthic macrofauna, presumably as a consequence of low and variable O_2 concentrations.

[12] Site 2 (for Case study 2) was located in Loch Etive, on the west coast of Scotland (56°27.33′N; 5°15.25′W). Loch Etive is a 30 km long glacial fjord with a narrow opening to the sea and two main sills dividing the fjord into two basins. This work was undertaken in the lower marine-dominated basin at ~55 m water depth. The O_2 concentration was relatively constant varying between 169–176 μM during the 56 h long deployment. However, the flow velocity measured at 12 cm off the seabed ranged between 0.3 and 12.6 cm s^{-1} as a consequence of tidal forcing. The sediment was cohesive mud and hosted a dense community of the brittle star *Amphiura filliformis*.

[13] At both sites, the velocity in the x, y, and z directions was sampled using a downward facing acoustic Doppler velocimeter (ADV) (Vector, Nortek, Norway), placed on a tripod frame. The ADV measuring volume (1.5×1.5 cm) was situated 20 and 12 cm above the seabed at Sites 1 and 2, respectively. O_2 concentrations were sampled at the edge of the ADV measuring volume using a pressure compensated Clark-type O_2 microelectrode [*Gundersen et al*., 1998; *Revsbech*, 1989] and a custom-built picoamperemeter, which was interfaced with the ADV electronics. Velocity and O_2 concentration were sampled with a frequency of 16 Hz (32 Hz at Site 2) in bursts of 15 min (14 min at Site 2) followed by a sleeping period of 15 min (1 min at Site 2). The O_2 microsensor was calibrated against zero and bottom water concentration using anoxic dithionite solution and the O_2 reading of an O_2 Optode (AADI, Norway) attached to a tripod deployed in parallel.

[14] At Site 1, approximately 300 m away from the EC system, a moored benthic-boundary-layer profiling system (BBL-Profiler) [*Holtappels et al*., 2011] was deployed. The BBL profiler consisted of a tripod frame that has a slide attached to one of the three legs. The slide was equipped with an O_2 optode (Model 4330, Aanderaa), a sensor measuring conductivity, temperature, and depth (CTD) (SeaCat, SBE, US) and an ADV (Vectrino Nortek, Norway). The slider moved vertically across the first 2 m above the sediment surface, stopping at programmed positions to measure for a time interval of 2 min. Prior to the deployment, the O_2 optodes were calibrated using dithionite solution and 100% saturated fresh water. The O_2 readings were corrected for salinity using equations from *Garcia and Gordon* [1992].

[15] For both sites, ADV and O_2 data from the EC system were processed using the following procedure: (1) velocities with a beam correlation of less than 50% were discarded and replaced by an average of the two neighboring values; (2) the data set was despiked using the method described by *Goring and Nikora* [2002]; (3) the tilt of the ADV was corrected using the planar fit method by *Wilczak et al*. [2001]; (4) the power spectral density and the cumulative cospectrum of the vertical velocity and the O_2 concentration was calculated [*Lorrai et al*., 2010]; (5) based on the cumulative cospectrum, which showed insignificant flux contributions below a frequency of 0.01 Hz, a running average with a window of 100 s was subtracted from the time series to calculate the fluctuating velocity w' and concentration C'; (6) the time series of w' and C' were cross-correlated for each burst allowing stepwise time shifts to a maximum 0.75 s of both, w' and C' [*Lorrai et al*., 2010; *McGinnis et al*., 2008], and the cross correlation with the highest correlation coefficient was used to calculate the flux; and (7) the cross correlations were subsequently evaluated by calculating the probability of receiving the same correlation (i.e., the same flux) from random data sets (corrcoef function in Matlab). The threshold for a significant flux was set to 5%.

3. Results

3.1. Case Study 1—Transient O_2 Concentrations

3.1.1. The Analytical Model

[16] For a known temporal change of O_2 concentration, the vertical flux can be calculated from equation (5). However, for a general analysis, it is more convenient to re-arrange equation (5) and introduce a proportionality factor R that depends only on the sensor position z and the dimensions of the logarithmic boundary-layer, i.e., z_0 and z_{up}. The

proportionality factor R is the ratio of the induced vertical flux (J) per temporal change of concentration ($\partial C/\partial t$):

$$R = \frac{J(z)}{(\partial C/\partial t)} = z\frac{\ln(z/z_{up})}{\ln(z_{up}/z_0) - 1} \quad (6)$$

[17] Using upper and lower estimates of z_o (10^{-3} and 10^{-5} m) and z_{up} (1 and 5 m), the range of the proportionality factor that can be expected at 15 cm above the sediment (the recommended position of the EC measuring volume) is calculated varying between −0.025 and −0.07 m (Figure 3). An increase of 10 μM O_2 h^{-1} would therefore result in a flux between −6.0 and −16.8 mmol O_2 m^{-2} d^{-1}, which is comparable to the O_2 uptake of typical shelf sediments. The negative sign indicates that the flux is directed towards the sediment. In contrast, decreasing O_2 concentrations would result in positive fluxes.

[18] From the field measurement, we estimated a bottom roughness (z_o) of 1×10^{-4} m by fitting the log-law (equation (4)) to the velocity profile of the BBL-profiler (Figure 4, left part). The upper boundary of the BBL (z_{up}) was assumed to be 2 m. The resulting proportionality factor R (Figure 4) decreases from zero at the lower and upper boundaries to −0.08 m at 70 cm above the sea floor. At 20 cm above the seafloor—the positions of the EC measuring volume at Site 1 (Black Sea)—the proportionality factor is still −0.05 m, and an increase of 10 μM O_2 h^{-1} results in a flux of −12.0 mmol O_2 m^{-2} d^{-1}.

3.1.2. Field Measurements

[19] During the 14 h of deployment, the average current velocities at Site 1 were varying between 5 and 9 cm s^{-1} (Figure 5a). A down-slope directed current carried O_2 concentrations, which increased on average by 1.2 μM h^{-1} (Figure 5B). However, the rate of change was not constant during the deployment. The change of O_2 over time was calculated for each burst by linear regression (Figure 5C), showing a strong increase of more than 4 μM h^{-1} in the first 2 h and between hour 8 and 11, whereas O_2 concentrations remain almost constant between hours 5 and 8. The O_2 flux from the EC measurement was calculated for each burst (Figure 5c). From a total of 27 bursts, two bursts were discarded due to insignificant correlation. The averaged O_2 flux of the remaining bursts was −6.0 mmol m^{-2} d^{-1}, which was greater than O_2 fluxes derived from microsensor

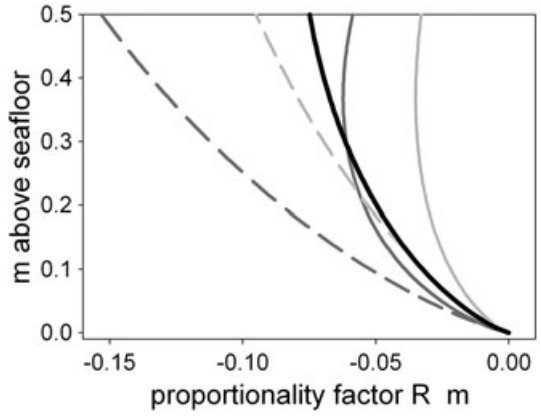

Figure 3. The proportionality factor (R) as a function of sensor position (z) and the following benthic boundary layer (BBL) dimensions: BBL height (z_{up}) of 1 m (solid lines) and 5 m (dashed lines) and roughness (z_0) of 10^{-5} m (light grey lines) and 10^{-3} m (dark grey lines). For Black Sea measurements, $z_0 = 10^{-4}$ and $z_{up} = 2$ m were assumed (black solid line).

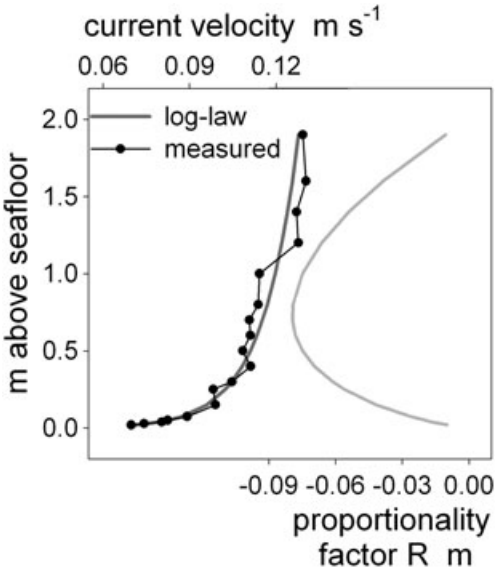

Figure 4. Black Sea deployment: left side: measured current velocity and fit with log-law. Right side: profile of R over the entire BBL of 2 m.

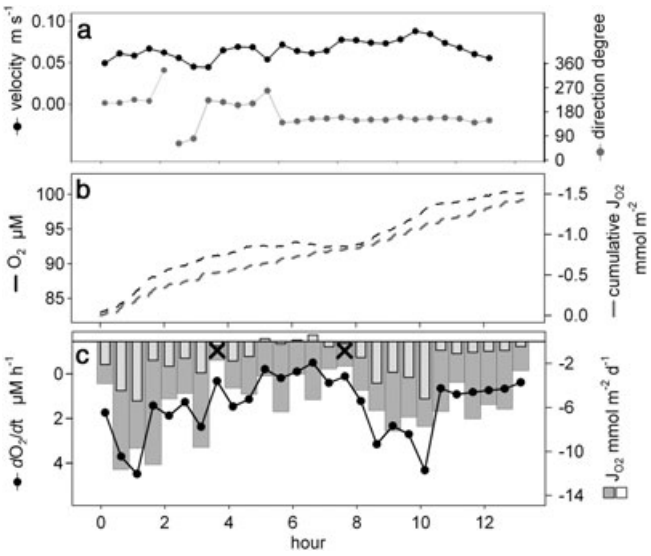

Figure 5. Results from the eddy correlation (EC)-measurement at the Crimean shelf, Black Sea show: (A) burst averages of current velocity and directions, (b) O_2 concentrations averaged over 100 s and the cumulative EC-flux, (c) the change of O_2 concentrations over time and the EC-flux, both averaged over the entire burst. The light grey bars in Figure 5C mark the O_2 flux induced by transient O_2 concentrations. Two bursts were discarded due to insignificant correlation (marked by **X**).

profiles ($-4.5 +/- 2.6$ mmol m^{-2} d^{-1}, $n = 7$) of a benthic lander at same station. Over the entire deployment, O_2 fluxes varied from -2.5 mmol m^{-2} d^{-1} to more than -11 mmol m^{-2} d^{-1}. Bursts with increased fluxes were found predominantly at times with strong O_2 increase, whereas decreased fluxes were found at times of constant or decreasing O_2. This is also observed when comparing the cumulative flux and the O_2 concentrations of individual bursts (Figure 5b), which show similar trends especially during the first 2 h and between hour 9 and 11. A significant linear relation ($p < 0.0005$) was found between the O_2 flux and the O_2 rate of change (Figure 6), which explains 42% of the O_2 flux variance. The slope of the linear regression, which gives the proportionality factor, was -0.05 m and matches the expected theoretical value (see above Figure 3, black line). The intercept of the linear regression (-4.2 mmol O_2 m^{-2} d^{-1}, Figure 6) gives the flux at steady state O_2 concentration, matching the O_2 flux derived from O_2-microsensor profiles. The flux due to changing O_2 concentrations was calculated from equation (5) and varied from +0.6 to -5.4 mmol O_2 m^{-2} d^{-1} (Figure 5c).

3.2. Case Study 2—Transient Current Velocities

3.2.1. The Numerical Model

[20] Two scenarios were simulated: accelerating and decelerating current velocities (Figure 7). The initial pressure gradient between the left and right boundaries of the model domain was adjusted to result velocities of 2 cm s^{-1} (and 10 cm s^{1}) at 15 cm above the lower boundary (Figures 7A and 7B). After simulating 3 h of steady state flow, the pressure gradient was readjusted to generate a 5 h increase (and decrease) of the velocity to 10 cm s^{-1} (and 2 cm s^{-1}). Thereafter, the velocity remained constant, and the flow returned to steady state. With changing velocities, the turbulent diffusivity (i.e., the turbulent viscosity) at the same depth varies between 0.4×10^{-4} and 2.2×10^{-4} m^2 s^{-1}. The transient conditions result in a phase shift between velocity and turbulent diffusivity. The initial increase of the turbulent diffusivity at hour 3 is delayed by 20 min compared to the initial velocity increase. Similarly, the turbulent diffusivity during deceleration is delayed by ~25 min. To follow the change during transient conditions, several vertical profiles

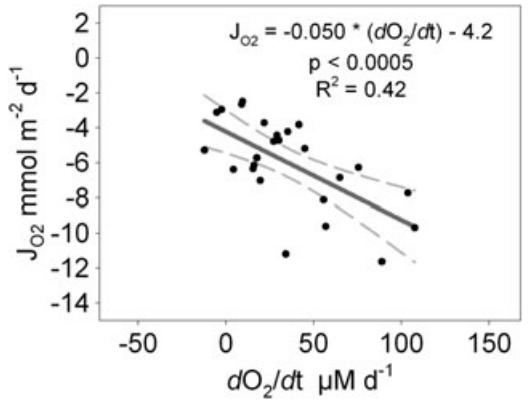

Figure 6. O_2 flux plotted against the change of O_2 concentration over time. The slope of the linear regression of -0.05 m gives an estimate of the proportionality factor *R*. Dashed lines mark the 95% confidence interval.

of current velocity, turbulent diffusivity, O_2 concentration and O_2 flux were extracted from the model (Figures 7c–7j).

[21] During accelerating flow, vertical gradients of velocity and turbulent diffusivity increase, whereas the vertical gradient of O_2 decreases (Figures 7c, 7e and 7g). The shear stress at the lower boundary is the source for the turbulent kinetic energy. Therefore, the initial increase of turbulent diffusion starts at the lower boundary and is moving upwards causing transient maxima in the center of the domain (Figure 7e), which disappear as the flow field reaches steady state. This evolution of the turbulent diffusivity causes an initial decrease of concentrations at depths close to the lower boundary, before concentrations gradually increase at all depths. Similarly, the downward flux of O_2 starts increasing at the lower boundary (Figure 7i) showing transient maxima that move upward and increase before they finally decrease and disappear as the flux returns to steady state at -10 mmol m^{-2} d^{-1}. The temporal evolution of the O_2 flux at 15 cm above the lower boundary (Figure 7a) shows a high initial flux of -17.5 mmol m^{-2} d^{-1} which is gradually decreasing to steady state conditions over the following 3.5 h. Further away from the boundary, the maximum flux increases up to -19.5 mmol m^{-2} d^{-1} (at 0.5 m) and remains high for several hours. Temporal integration of the deviating O_2-flux over the interval of transient conditions gives the total amount of excess O_2 per area that is transported between the layer above and below the depth of interest. At 0.15, 0.25 and 0.5 m, the integrated O_2 flux due to transient conditions is -0.36, -0.47 and -0.69 mmol m^{-2}, respectively.

[22] During decelerating flow, vertical gradients of velocity and turbulent diffusivity decrease, whereas the vertical gradient of O_2 increases (Figures 7d, 7f and 7h). Different from accelerating flow, velocity, diffusivity and O_2 concentrations are monotonic functions of time and space as they continuously decrease with time and towards the lower boundary. Compared to accelerating flow, the resulting deviation of the O_2 flux is less pronounced (Figure 7j) but lasts twice as long. The temporal evolution of the O_2 flux at 15 cm above the lower boundary (Figure 7b) shows a moderate decrease over 4 h to -7.1 mmol m^{-2} d^{-1} followed by a 4 h increase to steady state conditions. Further away from the boundary, the O_2-flux minimum is lowered to -6.7 mmol m^{-2} d^{-1} (at 0.5 m) and the return to steady state conditions is delayed by another 3 h. Temporal integration of the deviating O_2 flux over the interval of transient conditions is the same as for accelerating flow, but with opposite signs.

3.2.2. Field Measurements

[23] Field measurements at Loch Etive were used to study the effect of transient current velocities on the EC flux. During the total of 56 h of deployment, 4 periods of low and high tide were observed that correlated with a change in current direction and current velocities (Figures 8a and 8b). Each period lasted 12.5 h in which 2.5 h of high velocities (8.5–13 cm s^{-1}) and high EC fluxes (-20 to -60 mmol m^{-2} d^{-1}) (Figure 8d) were followed by 10 h of low velocities (1–3 cm s^{-1}) and low EC fluxes (0 to -20 mmol m^{-2} d^{-1}). The mean EC-flux over 4 tidal cycles (50 h) was -10.2 mmol m^{-2} d^{-1}. A standard deviation of $+/-11.1$ mmol m^{-2} d^{-1} illustrates the natural high variability of the EC-flux. Parallel to the EC measurements, O_2 microprofiles were measured

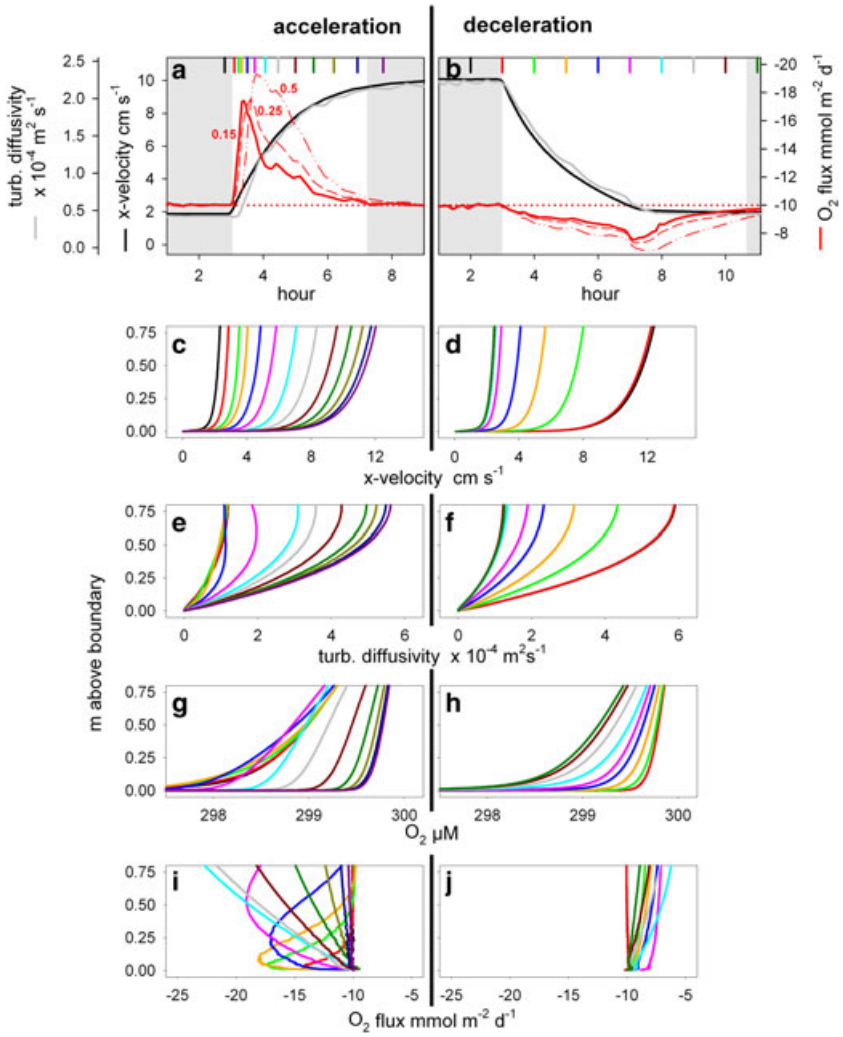

Figure 7. Results from the k-ε turbulent transport model show velocity, turbulent diffusivity and O_2-flux at 15 cm above the lower boundary during (a) accelerating and (b) decelerating flow conditions. The O_2-flux at 0 cm (dotted line), at 25 cm (dashed line) and at 50 cm (dashed-dotted line) above the lower boundary is also shown. Specific times are marked by colored bars in Figures 7a and 7b for which the vertical profiles of velocity (Figures 7c and 7d), turbulent diffusivity (Figures 7e and 7f), O_2 concentration (Figures 7g and 7h) and O_2-flux (Figures 7I and 7J) are shown.

using a transecting microprofiling instrument [*Glud et al*., 2009] and resolved a mean O_2 penetration depth of 3.7 +/− 1.1 mm ($n = 16$), a DBL thickness of 0.6 mm [*Inoue et al*., 2011] and a calculated average diffusive O_2 uptake of 7.9 +/− 1.2 mmol m^{-2} d^{-1}. Additionally, we deployed a benthic chamber lander right before and after the eddy measurement, and the chamber derived total O_2 uptake rates amounted to 10.4 and 16.8 mmol m^{-2} d^{-1}, respectively.

[24] During the EC deployment, O_2 concentration was relatively stable varying between 168 and 176 µM (Figure 8c). The change of O_2 over time ($\partial C/\partial t$) was calculated for each burst as described for the Black Sea data. However, the correlation between EC-flux and $\partial C/\partial t$ was weak, explaining less than 6% of the EC-flux variability. As such the flux due to transient O_2 concentrations was negligible, and on average, it amounted to −0.04 +/− 5 mmol m^{-2} d^{-1} (Figure 8c). The observed patterns of simultaneous increase and decrease of velocity and EC-flux, can be ascribed to several factors including changes in DBL resistance towards O_2 uptake, flow-induced shift in infauna behavior and flow dependent flushing of infauna burrows. However, it can also partly reflect an O_2-flux that deviates from the benthic O_2 uptake due to transient current velocities. To test this, we applied the numerical model and adjusted the input values for the pressure gradient to shorten the accelerating and decelerating intervals to 1 h (red line, Figure 8b). Upper and lower steady state current velocities were adjusted to 10 and 2 cm s^{-1}, respectively, which matches the measured current velocities over the first three tidal cycles. The measured average O_2-flux of the EC measurement (−10 mmol m^{-2} d^{-1}) and the average O_2 concentration (170 µM) were used as upper and lower boundary conditions. During acceleration, the modeled downward flux at the sensor position (12 cm above the lower boundary) increased by 100% up to −20 mmol m^{-2} d^{-1} and was elevated for 2.2 h. During deceleration, the flux decreased by 54% down to −4.6 mmol m^{-2} d^{-1} and was below the average flux for a total of 7 h. Temporal integration of the

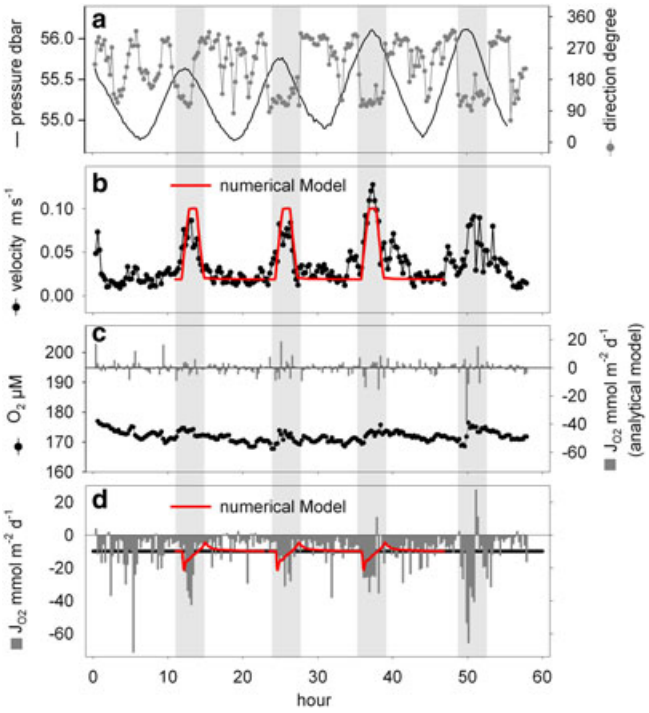

Figure 8. Results from the EC-measurement at Loch Etive show: (a) the pressure and current directions, (b) the current velocity, (c) the O_2 concentration and the estimated O_2-flux due to transient O_2 concentrations, (d) the EC-flux for each burst and the average EC-flux (black line). The total number of bursts was 231 of which five bursts were discarded due to insignificant correlation. Similar changes in current velocity were used in the k-ε transport model to estimate the O_2-flux at $z = 12$ cm (red lines).

deviating O_2 flux over the interval of transient conditions is the same for accelerating and decelerating flow, but with opposite signs. The modeled flux averaged over a full tidal cycle is therefore equal to the flux across the lower boundary (-10 mmol m^{-2} d^{-1}).

4. Discussion

[25] Both the analytical and the numerical model show that transient flow and O_2 concentrations can cause EC-fluxes that significantly deviate from the true flux across the sediment-water interface. For the case of transient O_2 concentrations it was possible to apply an analytical model because the flow field was constant and could be described by the log-law. However, the transient flow field in Case 2 results in phase shifts between velocity and turbulent diffusivity (Figures 7a and 7b), and transient maxima in turbulent diffusivity and O_2-flux profiles (Figures 7E and 7I), which are not reflected by analytical solutions derived from the log-law. Therefore, a k-ε turbulence model was necessary to capture the dynamics of turbulent transport across the BBL and the induced deviating EC flux. It should be mentioned that the flux across the sediment-water interface itself may show a temporal variability caused by, e.g., changing O_2 concentrations at the sediment surface, changing activity of the infauna or changing flushing rates in permeable sediments. However, in both models the variability of the flux across the sediment-water interface was neglected to allow an isolated examination of the potential errors due to transient conditions.

4.1. Case Study 1—Transient O_2 Concentrations

[26] The underlying assumption for the analytical model is a balance between differential advective transport and vertical diffusive transport (see equation (1)). This assumption may not be correct in case of abrupt changes of O_2 concentrations, which are occasionally recorded during EC measurements. To study how the balance is established after a sudden 5% increase of the O_2 concentration, we applied the COMSOL model and modified the following: (1) the domain was enlarged to 200 m length, 2 m height and 320,000 mesh elements; (2) in the k-ε module, a pressure difference between the left and right boundary was adjusted to a steady state velocity profile that matches the profile shown in Figure 4; (3) in the convection-diffusion model, the upper boundary was set to symmetry and the flux across the lower boundary was set to zero, and; (4) the inflow concentration at the left boundary was set to 105 µM, whereas the initial concentration in the domain was set to 100 µM. In this way, the evolution of a front with an abrupt 5% increase of O_2 concentration was modeled for 35 min using a time dependent solver. Figure 9 shows the temporal change of concentrations, the resulting downward flux and the proportionality factor, at 15 cm above the sediment and at different positions (20, 40, 80, 120, 160 and 200 m) downstream of the inflow boundary. The front slowly erodes as it propagates downstream (Figure 9A) and thus the maximum temporal change of O_2 concentration in the front decreases (Figure 9b) along with the induced vertical flux. The proportionality factor is approaching the theoretical value of -0.05 m as the front moves downstream (Figure 9C).

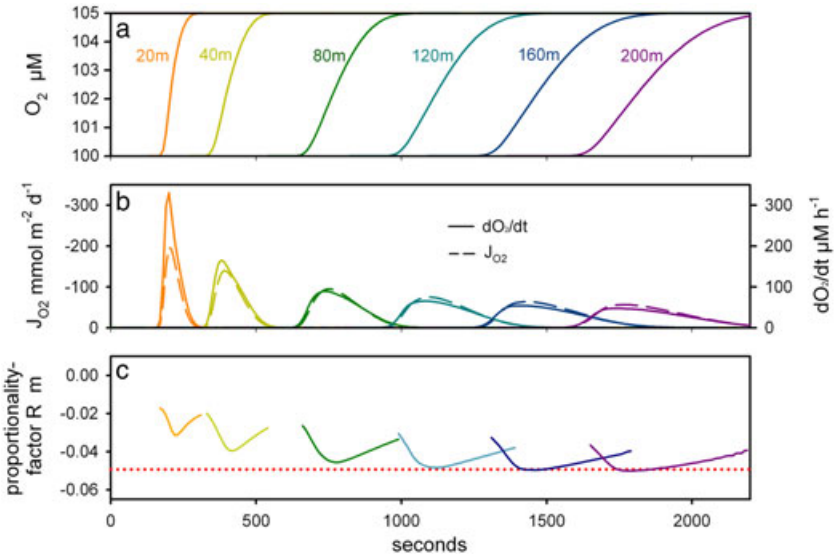

Figure 9. Results from a k-ε turbulent transport model simulating an abrupt increase of O_2 concentrations from 100 to 105 µM. The temporal change of (a) O_2 concentrations and (b) O_2 fluxes at 15 cm above the sediment is shown for different downstream-positions (color-coding). The (c) proportionality factor approaches the theoretical value of −0.05 m (red line) suggesting a balance between differential advective and vertical diffusive transport.

During the passage of the front at 200 m (i.e., 30 min after the initial change) the average value of the proportionality factor is −0.046 m (+/−0.004 m) suggesting that differential advective transport and vertical diffusive transport are nearly in balance. The numerical model shows that the analytical solution (equation (3)) is applicable already 30 min after the abrupt change of O_2 concentrations, which is, after all, an extreme nonsteady state situation causing extreme high vertical fluxes of up to −200 mmol m^{-2} d^{-1}.

[27] For the analytical model, we used the log-law to estimate the velocity profile and derive an exact solution that depends only on the boundary scales z, z_{up} and z_o. Strictly speaking, the log-law applies only for a specific layer within the entire boundary layer, but in many cases, it is also a reasonable model for the entire velocity profile (Figure 4). If the log-law is not applicable, which is the case in strongly stratified bottom waters [*Holtappels and Lorke*, 2011], equation (3) should be applied using measured current velocity profiles.

[28] Because the EC approach is based on the statistical analysis of two time series (i.e., the cross correlation of w′ and C′), statistical measures should be used to evaluate the calculated fluxes. We introduced a probability test of the cross correlation of w′ and C′ to estimate the probability of deriving the same correlation from completely random data sets with similar mean values and standard deviations. Using a threshold of 5%, the fluxes of two bursts at Site 1 were flagged as not significant (Figure 5c). From a total of 27 bursts, these two bursts gave the lowest flux (~2 mmol m^{-2} d^{-1}, $p < 0.14$) most likely defining the detection limit of the deployed EC system at the given conditions. However, rejecting flux estimates that are below the detection limit would bias the average flux towards higher values. On the other hand, non significant correlations are not necessarily caused by low or zero fluxes, but could result also from sensor failure or flow disturbances. Here, the calculated EC fluxes are compared with other factors such as the O_2 change over time (Figure 6). For this kind of analysis, non significant fluxes have to be discarded. In general, longer burst intervals would improve the probability of a significant correlation. For future deployments, we therefore recommend continuous measurements if sufficient power supply and data memory is at hand.

[29] After rejecting two bursts due to non significant correlation, the fluxes of the remaining bursts were analyzed in light of the transient O_2 concentrations. The ratio of EC fluxes to changing O_2 concentrations (i.e., the proportionality factor R) was predicted by the analytical model, and could explain 42% of the flux variance. The flux caused by increasing O_2 concentrations was significant. On average, 30% of the measured EC-flux could be attributed to transient O_2 conditions and for individual bursts proportions of up to 70% were found (Figure 5c). If mean O_2 concentrations would have decreased over time, the induced O_2 flux would have been positive and the superposition with the benthic O_2 uptake would have caused extremely low or even positive EC-fluxes, most likely below the detection limit. Applying equation (5) to correct the EC flux resulted in an average EC flux of −4.2 mmol O_2 m^{-2} d^{-1}, which matched the flux calculated from O_2 microsensor profiles. Given that the impermeable sediment contained no fauna, this alignment put confidence in the analytic approach.

[30] It is recommended to equip the EC systems with additional sensors that continuously record O_2, temperature and salinity to provide a robust and independent measurement of mean O_2 concentrations and to detect water masses of different origin. This is particularly important in shallow coastal waters where a high short-term variability of O_2 concentrations is to be expected. Additionally, ADCP measurements would help to determine the velocity profile

applied in equation (3) and help improve any corrections of EC-derived O_2 fluxes.

4.2. Case Study 2—Transient Current Velocities

[31] In general, the O_2-flux caused by transient current velocities depends on (1) the flux across the sediment water interface, (2) the acceleration/deceleration of current velocity and (3) the current velocity itself, as described in the following. The O_2-flux caused by transient current velocities is proportional to the O_2-flux across the sediment-water interface (see Figure 2). Doubling the O_2-flux across the lower boundary results in a doubling of the EC-flux deviation. Thus, the EC-flux deviation can be expressed in percent of the flux across the sediment-water interface. In the model study, accelerating and decelerating flow resulted in EC-flux estimates that deviated by +75% and −30% from the true flux across the sediment-water interface (Figures 7a and 7b). Adjusting the model to the conditions found at Loch Etive resulted in EC-deviations of up to +100%. Increasing acceleration/deceleration also increases the deviation of the flux. If the change in current velocity by 8 cm s^{-1} takes place twice as fast (i.e., from 2 to10 cm s^{-1} within 2.5 h instead of 5 h), the deviation of the EC-flux is doubled. The deviation will even increase further if the same acceleration/deceleration takes place at lower current velocities (e.g., between 0.5 and 8.5 cm s^{-1}). On the other hand, the deviation strongly decreases for acceleration/deceleration at high velocities.

[32] The results of the numerical model reflected the overall dynamic of the measured EC-fluxes at Loch Etive (Figure 8d). During peak periods, the transient flow conditions could explain considerable parts of the observed flux variation, but not all. It is not surprising that the benthic O_2 uptake is flow dependent; it has previously been documented that enhanced flow velocities stimulate passive flushing of infauna burrows [*Munksby et al*., 2002] and change infauna behavior and irrigation [*Vopel et al*., 2003]. Further, flow driven variations in DBL thickness can affect the O_2 uptake in coastal waters [*Glud et al*., 2007]. The increase of the O_2-flux upon complete elimination of the DBL can be calculated according to *Boudreau and Guinasso* [1982]. Applying the conditions found at Loch Etive and assuming depth independent volumetric O_2 consumption rates in the sediment, the theoretical elimination of the DBL would increase the O_2-flux only by a factor of 1.3, which does not explain the observed variability. In conclusion, the EC-resolved flow dependence of the O_2 uptake is confounded by transient flow phenomena as described above, and the remaining response must be ascribed to a combination of several factors as described above. However, the general alignment between average values for the EC derived flux, chamber incubations and microprofiles put confidence in the approach as long as data are carefully evaluated and assessed.

[33] The current study documents that quantitative flow responses as derived from EC-measurements should be evaluated with care. Transient flow velocities could explain a significant fraction of the variable EC-flux during tidal cycles. However, the modeled response reflected an asymmetric maxima and minima that cannot be resolved by the field data. We cannot exclude that other effects also could have contributed to the flux variability. For instance, periods of enhanced fluxes did also correlate with current direction (Figures 8a and 8d), and local disturbances of the flow field from obstacles located upstream during the time of high current velocities could have increased the turbulent mixing and there are indeed some hints suggesting this to be the case. At increased current velocities (direction 100°), time series of turbulent diffusivities calculated directly from the velocity fluctuations according to *Holtappels and Lorke* [2011] are above turbulent diffusivities calculated from the log-law, the latter assuming a steady state velocity field. At other times, the calculated diffusivities agree. This suggests a direction dependent imbalance of eddy diffusivities and the mean flow field, which could be explained by upstream located disturbances of the flow.

[34] It should be noted that fluxes due to transient conditions complicate other noninvasive measurements as well. The measurement of mean concentration gradients in the BBL [*Holtappels et al*., 2011] in combination with measured or calculated turbulent diffusivities [*Holtappels and Lorke*, 2011] are affected in the same way. However, the determination of relative fluxes of two different solutes (e.g., O_2 and NO_3^-) from their concentration profiles remains unaffected by nonsteady state current velocities, because the transient turbulent diffusivities are the same for both solutes [*Holtappels et al*., 2011].

4.3. Consequences for EC-Measurements

[35] Strong O_2 gradients and rapid change of current velocities in the bottom water are most likely found in coastal waters where winds, tides and strong O_2 sinks and sources prevail. Thus, EC-measurements under these conditions are challenging. We show that moderate changes of mean current velocities and mean O_2 concentrations can cause EC-fluxes that deviate by up to 100% from the true benthic flux estimate (Figure 8). In both cases, the discrepancy increases with the distance between the measuring volume and the seabed. Therefore, measurements closer to the sediment are less prone to errors than measurements conducted further away from the surface, but this will at the same time reduce the size of the measuring foot print. In general, it is recommended to carefully analyze the velocity and O_2 concentration time series recorded during EC-deployments and resolve their rate of change to estimate how this may confound the true benthic flux. In addition, we recommend EC-measurements over extended periods to cover the site-specific natural variability of flow conditions and O_2 concentrations. Long sampling periods increase the probability that biases due to increasing and decreasing velocities or concentrations are averaged out and result in a trustworthy mean flux.

[36] Interpretation of EC-fluxes is complex, and there is the risk of a biased selection between valuable data and outliers, since common objective evaluation criteria are not well defined, so far. In general, there is a priori no reason to discard extremely high or low fluxes that may not fit into the expected range, unless there is evidence that the sensor performances were compromised during those periods. Instead, the measured fluxes have to be interpreted in light of the present hydrodynamic conditions. This study provides some important guidelines to reach this ultimate goal.

Appendix A

[37] Applying the logarithmic law of the wall, the current velocity profile is calculated:

$$U(z) = \frac{u_*}{\kappa} \ln\left(\frac{z}{z_0}\right) \tag{A1}$$

[38] The depth averaged velocity $\bar{U}$ can be obtained by integration of the current velocity between z_0 and z_{up}, where z_0 denotes the hydraulic roughness and z_{up} the upper boundary of the BBL:

$$\bar{U} = \frac{1}{z_{up}} \int_0^{z_{up}} U(z)\mathrm{d}z = \frac{1}{z_{up}} \int_0^{z_{up}} \frac{u_*}{\kappa} \ln(z/z_0)\mathrm{d}z \tag{A2}$$

$$\bar{U} = \frac{1}{z_{up}} \frac{u_*}{\kappa} \left(\ln\left(z_{up}/z_0\right) z_{up} - \int_0^{z_{up}} z\mathrm{d}[\ln(z/z_0)] \right) \tag{A3}$$

$$\bar{U} = \frac{1}{z_{up}} \frac{u_*}{\kappa} \left(\ln\left(z_{up}/z_0\right) z_{up} - z_{up} \right) \tag{A4}$$

$$\bar{U} = \frac{u_*}{\kappa} \left(\ln\left(z_{up}/z_0\right) - 1 \right) \tag{A5}$$

[39] The flux due to changing concentrations over time is given by

$$J(z) = \frac{\partial C}{\partial t} \frac{1}{\bar{U}} \int_0^z U'(z)\mathrm{d}z \tag{A6}$$

[40] Equation (A-5) is inserted into equation (A-6):

$$J(z) = \frac{\partial C}{\partial t} \frac{1}{\bar{U}} \int_0^z (U(z)\text{-}\bar{U})dz \tag{A7}$$

$$J(z) = \frac{\partial C}{\partial t} \int_0^z (U(z)/\bar{U}\text{-}1)\mathrm{d}z \tag{A8}$$

$$J(z) = \frac{\partial C}{\partial t} \frac{1}{\ln\left(z_{up}/z_0\right) - 1} \int_0^z \left(\ln(z/z_0)\text{-}\ln\left(z_{up}/z_0\right) + 1\right)\mathrm{d}z \tag{A9}$$

$$J(z) = \frac{\partial C}{\partial t} \frac{1}{\ln\left(z_{up}/z_0\right) - 1} \left[\ln(z/z_0)z - z\text{-}\left(\ln\left(z_{up}/z_0\right) - 1\right)z\right] \tag{A10}$$

$$J(z) = \frac{\partial C}{\partial t} z \frac{\ln\left(z/z_{up}\right)}{\ln\left(z_{up}/z_0\right) - 1} \tag{A11}$$

Appendix B: COMSOL 2D Model

[41] Low-Reynolds-Number Turbulent Flow (k-ε) coupled to Transport of Diluted Species

Turbulent Flow, k-ε:

Domain:

Reynolds-averaged Navier-Stokes equations:

$$\rho \frac{\partial \mathbf{u}}{\partial t} + \rho(\mathbf{u}\cdot\nabla)\mathbf{u} = \nabla\cdot\left[-p\mathbf{I} + (\mu+\mu_T)\left(\nabla\mathbf{u} + (\nabla\mathbf{u})^T\right) - \frac{2}{3}\rho k\mathbf{I}\right] + \mathbf{F}, \rho\nabla\cdot\mathbf{u} = 0$$

Transport equation for turbulent kinetic energy k:

$$\rho \frac{\partial k}{\partial t} + \rho(\mathbf{u}\cdot\nabla)k = \nabla\cdot\left[\left(\mu + \frac{\mu_T}{\sigma_k}\right)\nabla k\right] + P_k - \rho\varepsilon$$

Transport for the dissipation rate ε:

$$\rho \frac{\partial \varepsilon}{\partial t} + \rho(\mathbf{u}\cdot\nabla)\varepsilon = \nabla\cdot\left[\left(\mu + \frac{\mu_T}{\sigma_\varepsilon}\right)\nabla\varepsilon\right] + C_{\varepsilon 1}\frac{\varepsilon}{k}P_k - C_{\varepsilon 2}\rho\frac{\varepsilon^2}{k}f_\varepsilon$$

with

turbulent viscosity $\mu_T = \rho C\mu \frac{k^2}{\varepsilon} f_\mu$

production term $P_k = \mu_T[\nabla\mathbf{u} : (\nabla\mathbf{u} + (\nabla\mathbf{u})^T)]$

damping functions

$$f_\mu = \left(1 - e^{-l^*/14}\right)^2 \cdot \left(1 + \frac{5}{{R_t}^{3/4}} e^{-(R_t/200)^2}\right)$$

$$f_\varepsilon = \left(1 - e^{-l^*/3.1}\right)^2 \cdot \left(1 + 0.3e^{-(R_t/6.5)^2}\right)$$

turbulent Reynolds number $R_t = \frac{\rho k^2}{\mu\varepsilon}$

dimensionless wall distance $l^* = \frac{\rho u_\varepsilon L_W}{\mu}$, with $u_\varepsilon = \left(\frac{\mu\varepsilon}{\rho}\right)^{1/4}$

closest wall distance $L_W = \frac{1}{G} - \frac{L_{ref}}{2}$, with $L_{ref} = 0.75$

constants $C_{\varepsilon 1} = 1.5$ $C_{\varepsilon 2} = 1.9$

$C_\mu = 0.09$ $\sigma_k = 1.4$ $\sigma_\varepsilon = 1.5$

dynamic viscosity $\mu = 0.001$ Pa s

density $\rho = 999.6$ kg m^{-3}

The reciprocal wall distance is solved:
$\nabla G \cdot \nabla G + \sigma_w G(\nabla\cdot\nabla G) = (1 + 2\sigma_w)G^4$, $\sigma_w = 0.1$

Boundaries:

Wall:

$$\mathbf{u} = 0 \quad k = 0 \quad \varepsilon = \lim_{L_W \to 0} \frac{2\mu k}{\rho {L_W}^2} \quad G = \frac{2}{L_{ref}}$$

Symmetry:

$$\mathbf{u}\cdot\mathbf{n} = 0 \quad \mathbf{K} - (\mathbf{K}\cdot\mathbf{n})\mathbf{n} = 0$$

$$\mathbf{K} = \left[(\mu+\mu_T)\left(\nabla\mathbf{u} + (\nabla\mathbf{u})^T\right) - \frac{2}{3}\rho k\mathbf{I}\right]\mathbf{n}$$

$$\nabla k\cdot\mathbf{n} = 0 \quad \nabla\varepsilon\cdot\mathbf{n} = 0 \quad \nabla G\cdot\mathbf{n} = 0$$

Periodic Flow Conditions

$\mathbf{u}_{source} = \mathbf{u}_{dest}$ $k_{source} = k_{dest}$

$\varepsilon_{source} = \varepsilon_{dest}$ $G_{source} = G_{dest}$

Pressure difference $p_{source} - p_{dest}$: manually adjusted

Transport of Diluted Species:

Domain:

Convection-Diffusion Equations

$$\frac{\partial c_i}{\partial t} + \nabla\cdot(-D_i\nabla c_i) + \mathbf{u}\cdot\nabla c_i = R_i$$
$$\mathbf{N}_i = -D_i\nabla c_i + \mathbf{u}c_i$$

with

Reaction rate $R_i = 0$
Turbulent + Molecular Diffusivity: $D_i = \frac{\mu_T}{\rho} + 10^{-9}\ \mathrm{m^2\ s^{-1}}$

Boundaries:

Periodic Conditions

$$c_{i,\mathrm{source}} = c_{i,\mathrm{dest}}$$

Flux

$$-\mathbf{n}\cdot\mathbf{N}_i = -1.1574\ x\ 10^{-7}\mathrm{mol}\ m^{-2}s^{-1}\left(=10\ \mathrm{mmol}\ m^{-2}d^{-1}\right)$$

Concentration

$$c_i = 0.3\ \mathrm{mol}\ m^{-3}(\mathrm{model\ study}), 0.17\ \mathrm{mol}\ m^{-3}(\mathrm{Loch\ Etive})$$

Mesh:

Number of mesh elements 36,250
Resolution at the wall: 0.00027 m

[42] **Acknowledgments.** The study was funded by the European Union's Seventh Framework Program HYPOX, Grant Agreement No 226213 coordinated by Antje Boetius. We thank Antje Boetius for organizing the Black Sea cruise (MSM 15/1). We are grateful to the crew of R/V *MS Merian* for their excellent support. R.N.G. and A.H. were supported by the National Environmental Research Council (NERC; NE/F018612/1; NE/F0122991/1, NE/G006415/1), the Commission for Scientific Research in Greenland (KVUG; GCRC6507) and European Research Council through an Advanced Grant (ERC-2010-AdG20100224). We thank Lars Umlauf and Christian Noss for their helpful comments and discussion.

References

Abe, K., T. Kondoh, and Y. Nagano (1994), A New turbulence model for predicting fluid-flow and heat-transfer in separating and reattaching flows .1. Flow-field calculations, *Int. J. Heat Mass Transfer*, *37*, 139–151.

Baldocchi, D. D. (2003), Assessing the eddy covariance technique for evaluating carbon dioxide exchange rates of ecosystems: past, present and future, *Global Change Biol.*, *9*, 479–492. doi:10.1046/j.1365-2486.2003.00629.x.

Berg, P., et al. (2003), Oxygen uptake by aquatic sediments measured with a novel non-invasive eddy-correlation technique, *Mar. Ecol. Prog. Ser.*, *261*, 75–83.

Berg, P., H. Røy, and P. L. Wiberg (2007), Eddy correlation flux measurements: The sediment surface area that contributes to the flux, *Limnol. Oceanogr.*, *52*, 1672–1684.

Boudreau, B. P., and N. L. Guinasso Jr (1982), The influence of a diffusive sublayer on accretion, dissolution, and diagenesis at the seafloor, in *The Dynamic Environment at the Ocean Floor*, edited by K. A. Fanning, and F. T. Manheim p. 115–145, Lexington, Mass.

Canfield, D., B. Thamdrup, and E. Kristensen (eds.) (2005), *Aquatic Geomicrobiology* pp. 129–166, Elsevier, San Diego, Calif.

Crusius, J., P. Berg, D. J. Koopmans, and L. Erban (2008), Eddy correlation measurements of submarine groundwater discharge, *Mar. Chem.*, *109*, 77–85. doi:10.1016/j.marchem.2007.12.004.

Fischer, H. B. (1979), *Mixing in Inland and Coastal Waters*, pp. 81–104, Academic Press, San Diego, Calif.

Garcia, H. E., and L. I. Gordon (1992), Oxygen solubility in seawater: Better fitting equations, *Limnol. Oceanogr.*, *37*, 1307–1312.

Glud, R. N., J. K. Gundersen, N. P. Revsbech, B. B. Jørgensen, and M. Huettel (1995), Calibration and performance of the stirred flux chamber from the benthic lander Elinor, *Deep-Sea Res. Part I*, *42*, 1029–1042.

Glud, R. N., P. Berg, H. Fossing, and B. B. Jørgensen (2007), Effect of the diffusive boundary layer on benthic mineralization and O_2 distribution: A theoretical model analysis, *Limnol. Oceanogr.*, *52*, 547–557.

Glud, R. N. (2008), Oxygen dynamics of marine sediments, *Mar. Biol. Res.*, *4*, 243–289. doi:10.1080/17451000801888726.

Glud, R. N., H. Stahl, P. Berg, F. Wenzhoefer, K. Oguri, and H. Kitazato (2009), In situ microscale variation in distribution and consumption of O2: A case study from a deep ocean margin sediment (Sagami Bay, Japan), *Limnol. Oceanogr.*, *54*, 1–12.

Glud, R. N., et al. (2010), Benthic O_2 exchange across hard-bottom substrates quantified by eddy correlation in a sub-Arctic fjord, *Mar. Ecol. Prog. Ser.*, *417*, 1–12. doi:10.3354/meps08795.

Goring, D. G., and V. I. Nikora (2002), Despiking acoustic Doppler velocimeter data, *J. Hydraul. Eng.-Asce*, *128*, 117–126. doi:10.1061/(asce)0733-9429.

Gundersen, J. K., N. B. Ramsing, and R. N. Glud (1998), Predicting the signal of O_2 microsensors from physical dimensions, temperature, salinity, and O_2 concentration, *Limnol. Oceanogr.*, *43*, 1932–1937.

Holtappels, M., M. M. M. Kuypers, M. Schlueter, and V. Bruechert (2011), Measurement and interpretation of solute concentration gradients in the benthic boundary layer, *Limnol. Oceanogr.-Methods*, *9*, 1–13. doi:10.4319/lom.2011.9.1.

Holtappels, M., and A. Lorke (2011), Estimating turbulent diffusion in a benthic boundary layer, *Limnol. Oceanogr.-Methods*, *9*, 29–41. doi:10.4319/lom.2011.9.29.

Huettel, M., W. Ziebis, and S. Forster (1996), Flow-induced uptake of particulate matter in permeable sediments, *Limnol. Oceanogr.*, *41*, 309–322.

Hume, A. C., P. Berg, and K. J. McGlathery (2011), Dissolved oxygen fluxes and ecosystem metabolism in an eelgrass (Zostera marina) meadow measured with the eddy correlation technique, *Limnol. Oceanogr.*, *56*, 86–96. doi:10.4319/lo.2011.56.1.0086.

Inoue, T., R. N. Glud, H. Stahl, and A. Hume (2011), Comparison of three different methods for assessing in situ friction velocity: A case study from Loch Etive, Scotland, *Limnol. Oceanogr.-Methods*, *9*, 275–287, doi:10.4319/lom.2011.9.275

Johnson, K. S., J. P. Barry, L. J. Coletti, S. E. Fitzwater, H. W. Jannasch, and C. F. Lovera (2011), Nitrate and oxygen flux across the sediment-water interface observed by eddy correlation measurements on the open continental shelf, *Limnol. Oceanogr.-Methods*, *9*, 543–553. doi:10.4319/lom.2011.9.543.

Jørgensen, B. B., and N. P. Revsbech (1985), Diffusive boundary layers and the oxygen uptake of sediments and detritus, *Limnol. Oceanogr.*, *30*, 111–122.

Loescher, H. W., B. E. Law, L. Mahrt, D. Y. Hollinger, J. Campbell, and S. C. Wofsy (2006), Uncertainties in, and interpretation of, carbon flux estimates using the eddy covariance technique, *J. Geophys. Res.-Atmos.*, *111*, D21S90, doi:10.1029/2005JD006932.

Long, M. H., D. Koopmans, P. Berg, S. Rysgaard, R. N. Glud, and D. H. Sogaard (2011), Oxygen exchange and ice melt measured at the ice-water interface by eddy correlation, *Biogeosciences*, *9*, 1957–1967. doi:10.5194/bg-9-1957-2012.

Lorke, A., B. Muller, M. Maerki, and A. Wüest (2003), Breathing sediments: The control of diffusive transport across the sediment-water interface by periodic boundary-layer turbulence, *Limnol. Oceanogr.*, *48*, 2077–2085.

Lorrai, C., D. F. McGinnis, P. Berg, A. Brand, and A. Wüest (2010), Application of oxygen eddy correlation in aquatic systems, *J. Atmos. Oceanic Technol.*, *27*, 1533–1546. doi:10.1175/2010jtecho723.1.

McGinnis, D. F., P. Berg, A. Brand, C. Lorrai, T. J. Edmonds, and A. Wüest (2008), Measurements of eddy correlation oxygen fluxes in shallow freshwaters: Towards routine applications and analysis, *Geophys. Res. Lett.*, *35*, L04403, doi:10.1029/2007GL032747.

Munksby, N., M. Benthien, and R. N. Glud (2002), Flow-induced flushing of relict tube structures in the central Skagerrak (Norway), *Mar. Biol.*, *141*, 939–945. doi:10.1007/s00227-002-0874-x.

Reimers, C. E., H. T. Oezkan-Haller, P. Berg, A. Devol, K. McCann-Grosvenor, and R. D. Sanders (2012), Benthic oxygen consumption rates during hypoxic conditions on the Oregon continental shelf: Evaluation of the

eddy correlation method, *J. Geophys. Res.-Oceans*, *117*, C02021. doi:10.1029/2011JC007564.
Revsbech, N. P. (1989), An oxygen microsensor with a guard cathode, *Limnol. Oceanogr.*, *34*, 474–478.
Taylor, G. I. (1938), The spectrum of turbulence, *Proc. R. Soc. A*, *164*, 476–490.
Taylor, G. I. (1953), Dispersion of soluble matter in solvent flowing slowly through a tube, *Proc. R. Soc. Lond. A Math. Phys. Sci.*, *219*, 186–203.
Thamdrup, B., and D. Canfield (2000), Benthic respiration in aquatic sediments, in *Methods in Ecosystem Science*, edited by O. Sala, H. Mooney, R. Jackson, and R. Howarth, pp. 86–103, Springer, New York.
von Karman, T. (1930), Mechanische Ähnlichkeit und Turbulenz, pp. 85–105, Proceedings of the Third International Congress of Applied Mechanics.
Vopel, K., D. Thistle, and R. Rosenberg (2003), Effect of the brittle star *Amphiura filiformis* (*Amphiuridae*, *Echinodermata*) on oxygen flux into the sediment, *Limnol. Oceanogr.*, *48*, 2034–2045.
Wenzhöfer, F., and R. N. Glud (2002), Benthic carbon mineralization in the Atlantic: A synthesis based on in situ data from the last decade, *Deep-Sea Res. I*, *49*(7), 1255–1279.
Wilczak, J., S. Oncley, and S. Stage (2001), Sonic anemometer tilt correction algorithms, *Boundary-Layer Meteorol.*, *99*, 127–150.